Macromolecules **2021** *54* (9), 4164-4175, DOI: 10.1021/acs.macromol.1c00515

Effect of Nanofiller's Size on the Mechanical Properties of Poly(acrylic acid)/Graphene Oxide Nanocomposites

Georgios Kritikos and Kostas Karatasos*

Laboratory of Physical Chemistry, Department of Chemical Engineering, Aristotle University of Thessaloniki, 54124, Thessaloniki, Greece.

Abstract: Two poly(acrylic acid) (PAA)/graphene oxide nanocomposite systems, characterized by the same graphene oxide (GO) weight fraction (13.5 wt %), but with different size of the nanoflakes, are studied by means of molecular dynamic (MD) simulations and the solid to liquid glass (SLG) transition model. The MD density data were described well by the SLG equation of state (SLG-EoS) and the PAA thermal expansion coefficient was predicted to decrease with the size of the GO nanosheets. A new equation for the description of the bulk modulus is introduced and used for the estimation of the effects of the size of the GO flakes on the mechanical properties of the composites. The mechanical behavior of the composites was found to depend on the size of

the GO filler. In the case of larger in size GO flakes, the chains form longer sequentially adsorbed configurations (trains) as well as loops, while in the presence of smaller in size GO nanoflakes, the train configurations are shorter, and the polymer bridging is extensive. The slow mobility of the large GO flakes, results in more retarded dynamics of the PAA chains, explaining the higher viscosity and the enhanced mechanical properties compared to the small GO system. Furthermore, using a generalized Arrhenius equation (SLG model), the dynamic behavior at high temperatures is extrapolated to the glass transition region, providing thus a means to describe dynamics at lower temperatures. Analysis of the configuration-specific bound layer polymer dynamics, in hydrogen-bond forming systems, reveals that chain immobilization is restricted to a layer surrounding the nanofiller, rather than propagating in a way that would promote the formation of "glassy bridges" between nanofillers.

Introduction

Understanding the morphological characteristics, the extent and the motional behavior of the bound polymer layer, is essential for the elucidation of the dynamic and mechanical response in polymer nanocomposites. Over the last 50 years, experiments focusing on the properties of carbon-based polymer nanocomposites,[1–3] detected the modification of the polymer dynamics due to the presence of the polymer/solid interface.[4–14] In a typical Dielectric Relaxation Spectroscopy (DRS) experiment[13,14] the formation of such a layer is revealed through the peculiar Arrhenius-like segmental dynamics close to the polymer/filler interface, while the non-adsorbed polymer fraction exhibits a pronounced departure from the constant activation energy trend (super-Arrhenius

behavior). The distinct bound layer segmental process has been called α',[11,15] in contrast to the commonly studied bulk segmental motion, referred to as the α mechanism.

The suppression of the dielectric strength, due to the immobilization of the active dipoles and the reduced heat capacity step in Differential Scanning Calorimetry (DSC) experiments,[13,16–19] due to the constrictions imposed in polymer configurational degrees of freedom, are considered as a signature of the bound layer transition[9,16,18,20,21] to a "dead" or "glassy" layer, also termed as a rigid amorphous fraction (RAF)[19] or rigid amorphous phase (RAP),[22] formed around the nanoparticles. The RAP is also present in polymers forming a crystalline phase (CP).[16,19,23–25] The stabilization[13,16,24] of the fraction of mobile amorphous phase (MAP) at the glass transition temperature (T_g) in amorphous and semicrystalline polymer nanocomposites, independently of the filler content, poses challenging questions regarding the nature of polymer semi-crystallization and the glassy behavior close to interfaces.

So far, we know that a bound polymer layer forms when strong polymer/filler interactions are present.[9,16,18,20,21] In this layer, local polymer dynamics is decoupled from the rest MAP fraction[9,16,18,20,21,26] (i.e. follows an Arrhenius-like behavior). In case of semicrystalline polymer nanocomposites[16] it is less affected by the cooling rate compared to the CP and it undergoes a "stronger" transition to a RAP at a temperature almost 100 K above the T_g.[9,16,18,20,21] The bound layer transition is characterized by a smother reduction of the entropy,[16] that is verified by the absence of a clear heat capacity step.[16] In some cases, a shielding/cloaking effect[16,27,28] can be observed, which is responsible either for a minor increment in the T_g or even no increase at all.[13,14,17,24,29,30] The dynamic behavior within the bound layer may exhibit different anisotropic characteristics depending on the nanosheet roughness.[28] Moreover, the formation of this layer has been associated with enhanced mechanical properties.[2,6,18,31–35]

The observed mechanical reinforcement process in polymer nanocomposites few degrees above the pristine polymer T_g,[32,36] has been attributed to two different mechanisms. One mechanism assumes[31] a network of (solid phase) nanofillers, whose deformation justifies increased values of the bulk, elastic and shear modulus. Another approach proposes the formation of immobilized, glassy polymer bridges between different nanofillers, in extreme confinement conditions,[32,33,37] that resist to deformation. In the latter mechanism, strong polymer/nanofiller interactions, e.g., hydrogen bonding, are necessary to be present. This approach is also consistent with the existence of a distribution of T_gs.[6,34,35,38]

The aforementioned mechanisms, however, do not provide information as to the role of the spatial distribution of the immobilized polymer fraction close to the polymer/filler interface and how this is reflected to the mechanical properties of the composites. In the case of graphene-based polymer composites, although the TPa scale modulus[3] of a graphene sheet could partly account for the observed enhanced mechanical properties, other aspects of this enhancement remain to be clarified. For instance, experimental studies on graphene platelets revealed different stress transfer mechanisms depending on the size of the nanosheet,[2] while bound layer polymer dynamics was found to be affected by the nanofiller size.[39] Therefore, further investigation on the role of the characteristics of the adsorbed polymer layer in the observed mechanical response in polymer/graphene nanocomposites, needs to be performed.

The bound layer morphological characteristics have mainly been described by the use of Molecular Dynamic (MD)[8,10,28,40,41] and Monte Carlo (MC)[42–44] simulations, in addition to numerical Self Consistent Mean Field methods.[16,45] Among them, fully atomistic MD simulations have been proved invaluable for the description of pertinent length and timescales (within the simulation window) involved in the dynamic phenomena within the bound layer. On the other

hand, these studies cannot extent to timescales close to the longest relaxation times involved in the bound layer dynamics. A way to overcome this restriction is through the use of theoretical extrapolation tools. One example is the classical Vogel-Fulcher-Tammann (VFT)[46–48] equation, $\tau = \tau_o exp\left[\frac{B}{T}\left(\frac{T}{T-T_o}\right)\right]$, were τ_o is a preexponential factor, B is the activation energy and T_o is the so-called Vogel temperature. Although this relation is successful in describing the super-Arrhenius increase in the activation energy, it fails in some other aspects. For example, it cannot describe the transition to the Arrhenius region at temperatures much higher than T_g,[49–51] it does not comply with the Arrhenius behavior observed in lower than T_g temperatures,[52] the evaluated B is not in agreement with the one describing the sub-T_g region,[51] while it also introduces a diverging temperature (T_o) that is not compatible with the aging process[5,7] below T_g.[51,53,54]

To address those deficiencies, a generalization of the Arrhenius equation has recently been proposed.[51,55] Since a diverging temperature is consistent with the first order liquid to solid transition, it is reasonable to assume that an additional component in the classical Arrhenius equation is also required. Along these lines, this component (g), which has been associated to a sigmoidal switching function of the cohesion energy, incorporates an extension parameter δ_g (temperature units) and a characteristic temperature parameter, which for generalization purposes can be identified as the T_g. By defining, $g = exp\left(\frac{T_g - T}{\delta_g}\right)$, the new equation takes the form:

$$\tau = \tau_o exp\left(\frac{B}{T}\left[1 + exp\left(\frac{T_g - T}{\delta_g}\right)\right]\right) \quad (1)$$

It has been shown[51,56] that by extending the solid to liquid transition region (parameter δ_g), the glass transition dynamical and structural phenomenology can be described in a unified manner. Moreover, the entire super-Arrhenius region in polymer nanocomposites can be followed by one

T_g parameter, while the Arrhenius-like behavior of the bound layer can be interpreted by increased values of the δ_g parameter (of the order of 100 K).

In this article, we present a MD simulation comparative study of two different poly(acrylic acid)/graphene oxide, (PAA/GO) nanocomposites, which are characterized by the same weight percentage (wt%) in GO, but different size nanosheets. The two new elements that this study introduces are: a) assessment of the effect of the nanosheet's size on the viscosity/mechanical behavior of the nanocomposites, when the extent of the polymer/solid interface is kept constant and b) description of dynamics (bound layer immobilization process), thermodynamics and mechanical properties using a new EoS-based methodology. In the next section we provide a brief description of the simulation protocol of the PAA/GO systems which has been presented in more detail in previous investigations of the same models.[28,57] The results and discussion section follows, presenting the analysis and discussing the findings of the MD simulations. We conclude with the main points of the study and future plans.

Simulation Details

Two PAA/GO systems were simulated, characterized by a constant GO weight percentage of 13.5 wt%, which is in the range of filler contents studied experimentally.[57,58] One system contained 7 small GO nanosheets, with dimensions of 1.5 x 2 nm^2 embedded in a polymer matrix of 32 PAA chains each comprised by 40 monomers. In this case the dimensions of the GO flake were close to the dimensions of a PAA chain ($R_g \approx 1.4$ nm).[57] The second system consisted of one GO nanosheet, having initial dimensions of 9 x 8.4 nm^2, in a matrix of 90 PAA chains with 40 monomers each. In terms of volume fraction, the GOs occupied on average, almost 50 % of the system's volume. The GO nanosheet was characterized in both cases by a carbon to oxygen atom ratio of 5:1 and a hydroxyl to epoxy group ratio of 3:2 approximately, as described in previous works.[28,55,57,59] The

first system is labeled as PAAsGOhwt and the second system as PAAGOhwt. In some cases, we have compared the results with a previous system,[28] where the same large GO nanosheet was included in a matrix of 1300 PAA chains (1.0 wt%) and is labeled as PAAGOlwt. Also, a bulk system of 50 PAA chains with 40 monomers each (bulkPAA) was used as a reference.

The all atom representation of the PAA/GO nanocomposites was described with the use of the AMBER forcefield.[60,61] The Gromacs package[62] was employed and the simulations were performed with the isothermal-isobaric (NPT) ensemble, using the velocity-rescale thermostat[63] and the Berendsen barostat.[64] The box dimensions, at the highest temperature, were almost 5.5 x 5.5 x 5.0 nm^3 and 10.1 x 10.1 x 3.9 nm^3 for the PAAsGOhwt and PAAGOhwt systems, respectively. The larger nanosheet was inserted parallel to the x,y plane of the simulation box. In both cases, polymer bridges can be formed, as, even in the large GO system, the short dimension was taken close to the end-to-end distance of the PAA.

Dynamics were probed at the pressure of 0.1 MPa, in the region between 500 to 700 K with a step of 50 K. Also, lower temperatures down to 300 K, with the same temperature step, were simulated in order to derive the density-temperature dependence above and below T_g. Furthermore, equilibration runs of the order of 100 ns were applied successively in both systems, during the cooling process, at each temperature. Especially in the PAAsGOhwt system, where the initial configuration was taken from a previous simulation study on a similar system,[57] the total equilibration time lasted 500 ns, before the final equilibrium distribution of the small nanosheets was reached. After that, production runs from 500 ns to 1 μs, depending on the longest relaxation time at each temperature, were performed.

Results and Discussion

The investigation of the bound layer dynamics involves relaxation times that almost 100 K above the T_g, reach the order of μs and cannot be easily probed by atomistic MD simulations. In order to approach this region, in this study the SLG model is employed. According to the model, as the temperature drops there is a critical temperature value (T_A or T_{cr}), related to a critical value of the segmental free volume (v_{cr}^{free}), below which the relaxation times do not follow the Arrhenius equation. Due to the lack of the necessary free volume,[65,66] a fraction f_1 of the macromolecular segments undergoes a transition to a bound state (with energy level T_1^*), so that the rest mobile fraction f_2 continues occupying the liquid state (with energy level T_2^*), justifying an Arrhenius component in the diffusion. It is also assumed that a total fraction (f_1') of the system participates in the transition process between the two states, so that the rest part continues diffusing in a Brownian fashion. Following this picture, there will be another critical temperature, where $f_1' = 1$ (percolation threshold) and the cooperative diffusion will cease. We identify this temperature as the T_g. To describe this bimodal process (eq.1), an additional term (g) needs to be added into the Arrhenius equation, which expresses the balance between the bound and the liquid states, i.e. $g = {f_1}/{f_2}$. The only way that g goes to unity at T_g (beyond this value only the Arrhenius component is accessible), is to assume that the bound state is the solid state of zero free volume. According to this approach, at T_g, all segments undergo a solid to liquid transition, exchanging free volume ($f_1' = 2f_1$).[51]

The description of the transition regime is realized through two parameters, namely the T_g temperature and the parameter δ_g. The latter is related to the extension of the super-Arrhenius region and the fragility[67] of the glass transition. Then the solid-state fraction is determined[51] to follow a sigmoidal function of the form, $f_1 = 1/\left(1 + exp\left(\frac{T-T_g}{\delta_g}\right)\right)$. Furthermore, the cohesion

energy in the super-Arrhenius region can be described by an equation of the form, $T^* = T_2^* + f_1(T_1^* - T_2^*)$. In terms of the Flory-Huggins (FH) theory,[68,69] the mean-field parameter ($\chi = \frac{T^*}{T}$) can be calculated by:

$$\chi = \chi_2 + f_1(\chi_1 - \chi_2)\,, \tag{2}$$

where $\chi_2 = {}^{T_2^*}/_{T}$ and $\chi_1 = {}^{T_1^*}/_{T}$ are the FH parameters at the liquid and the solid state respectively. In the framework of the FH theory, χ parameter is generally accepted[70,71] to be consisted by two terms, one of enthalpic and another one of entropic origin. In our extension of the mean field, the additional second term is related to the probability to find a segment in the solid state compared to the probability to find it in the liquid state.[56] Introduction of this temperature dependence of the mean-field into the Sanchez-Lacombe (SL) theory,[72] leads to the derivation of a new description of the Helmholtz free energy (*F*), as shown is eq. s1 of the supporting information (SI) section. At equilibrium, each term of *F* should be minimized, and this determines the size of the solid state phase, in amorphous polymers, to be as small as possible.[56] So, we may identify the fraction f_1 to be consisted of "droplets of solid state". In the framework of the same model, the SLG-EoS can be derived as:

$$\frac{Pv}{kT} + \left(1 - \frac{1}{r}\right)\tilde{\rho} + ln(1 - \tilde{\rho}) + \chi\tilde{\rho}^2 = 0 \tag{3}$$

where *P* is the pressure, *v* is the segmental volume at the solid state, *r* is the degree of polymerization, *k* is the Boltzmann constant, $\tilde{\rho} = {}^{\rho}/_{\rho_o}$ and ρ, ρ_o are the densities at the temperature *T* and at the solid state respectively.

The idea of the existence of droplets of solid state (structural heterogeneity) in the super-Arrhenius region,[16] whose fraction increases in a sigmoidal fashion with the temperature reduction, has been supported by a recent work,[73] while another theoretical approach for the description of

local dynamics and glass transition phenomena, has also been extended to adopt a temperature dependence of relaxation times, similar to that of eq 1.[74]

Thermodynamics and Structure.

Figure 1 illustrates, typical configurations of PAA chains confined by GO nanoflakes of two different sizes. It is worth mentioning that in the PAAsGOhwt system the formation of continuous clusters (driven by filler-filler interactions[31]) of GO flakes, that could resist to the deformation, justifying a solid-like behavior of the elastic modulus, in principle could have been detected by the MD simulations. However, despite the long runs (of the order of μs) no such instance was observed. Instead, a kind of phase separation between the small GO flakes and the PAA chains seems to be favored. In both systems, the adsorbed polymer chains assume various configurations, such as trains, loops, tails and bridges. In Figure S2 of SI, snapshots of the entire systems are presented.

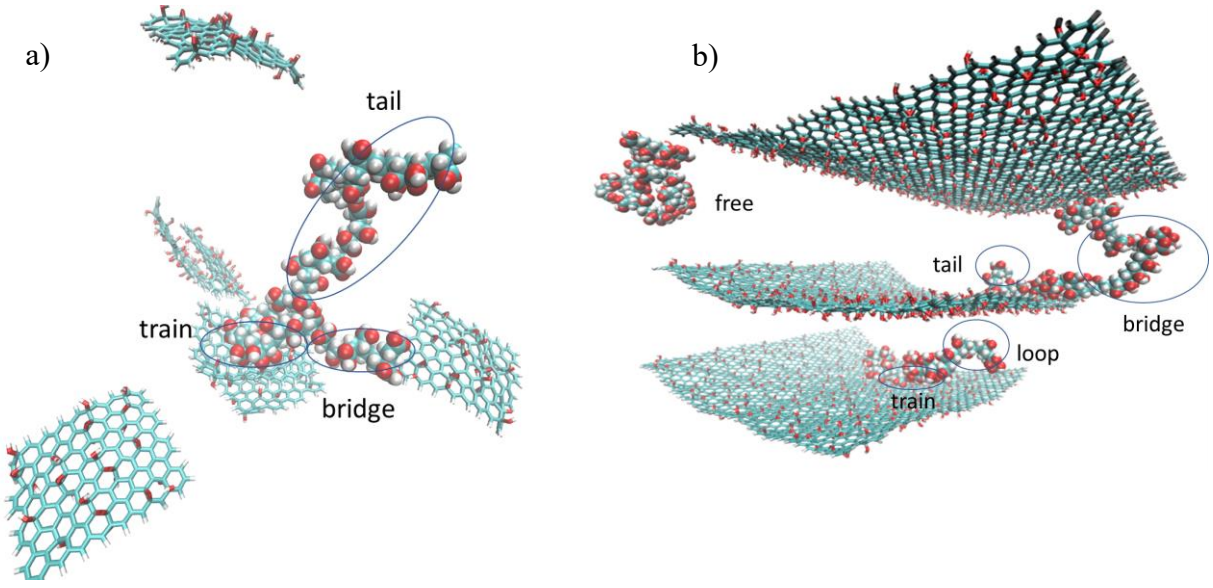

Figure 1. Snapshots[75] of confined PAA chains in a) PAAsGOhwt and b) PAAGOhwt systems. In case of the second system periodic images are also included. The possible bound layer configurations (trains, loops, tails and bridges) and free chains are circled. Other neighboring polymer chains are omitted for clarity.

Figure 2 shows the normalized (with respect to the corresponding bulk value) density profiles of PAA as a function of the distance from the GO surface for both the PAAsGOhwt and the PAAGOhwt systems. We have used the same coordination system as the one described in previous studies.[28,76] It is shown that the density fluctuations, near the GO surface, are present in both systems, while in the system consisting of seven small flakes, the first peak is lower in amplitude compared to the same peak at the large GO system. This can be explained by the self-assembly of GO flakes (Figure 1), that may exclude polymer chains from the surface, resulting in reduced average polymer density values. The distance corresponding to the first minimum in the density profile, was used to define the width of the adsorbed layer. Therefore, when an atom's vertical z distance from the nanosheet is shorter than the adsorbed layer's width and its projection on the xy-plane lays on the GO, it is considered to be in the adsorbed state. A chain having at least one of its atoms adsorbed, is taken to be adsorbed and free otherwise. Furthermore, the limiting case of inter-sheet distance, where no middle layer with bulk density is observed,[40] is defined as extreme confinement condition. Due the chosen filler content, such a case is present in the PAAGOhwt system and can be observed in some situations in the PAAsGOhwt system, as well.

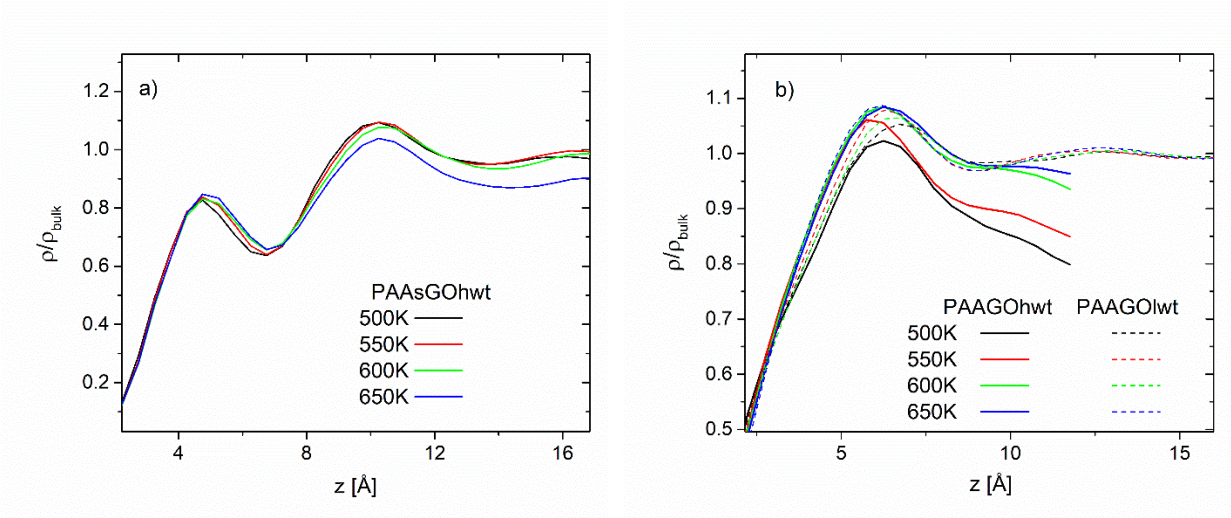

Figure 2. Normalized density profiles for the a) PAAsGOhwt and b) PAAGOhwt and PAAGOlwt systems.

Figure S3 of SI compares the temperature dependence of the density for the bulk PAA, the PAAsGOhwt and the PAAGOhwt systems. As can be seen, the density values obtained from the NPT runs for all the systems, can be accurately described by the SLG-EoS (eq. 3).[55,57]

Knowledge of the temperature dependence of the density allows the derivation of the bulk modulus, as the inverse of the isothermal compressibility, $K = \left(\frac{1}{\tilde{\rho}}\frac{\partial\tilde{\rho}}{\partial P}\right)^{-1}$. Combined with eq. 3, K can be calculated by the following relation:

$$K = kT\frac{1}{v}\left(\tilde{\rho}\left(\frac{1}{1-\tilde{\rho}}\right) - \tilde{\rho}\left(1-\frac{1}{r}\right) - 2\chi\tilde{\rho}^2\right) \quad (4)$$

In this form the term $\partial\chi/\partial P$ has been neglected, since the pressure dependence of the T_g ($\partial T_g/\partial P$) was considered to take small values, around 0.1 K/MPa.[77] Eq. (3) is compatible with the experimental observation of improved mechanical properties, above the T_g, as the parameter δ_g increases.[13,32,51,55] Moreover, with the use of the Poisson's ratio (μ),[77] the elastic (E) and shear (G) moduli can also be calculated ($E = 2G(1+\mu) = 3K(1-2\mu)$), allowing thus a complete

mechanical characterization of a glassy material, avoiding artifacts involved in MD simulations (e.g. close to linear temperature dependence of E[55,78]).

In Figure 3, the bulk modulus values of each system, as evaluated by the fluctuations of the simulation box volume (V), in the NPT runs, are shown as empty symbols, ($K = kT\frac{\langle V\rangle}{\langle V^2\rangle-\langle V\rangle^2}$). To determine the optimum parameters (Table S1 of SI) that best describe the simulation data in Figure 3 and in Figure S2 of SI, a minimization process for both eqs. 2 and 4 took place simultaneously, for each system. In agreement with the bulk modulus data collected by the NPT runs, the SLG methodology predicted enhanced mechanical properties for both nanocomposite systems (solid lines in Figure 3), with the PAAGOhwt exhibiting the highest K values. Moreover, the T_g and δ_g parameters were determined (Table S1 of SI) to be, 435 K and 31 K, 460 K and 31 K and 471 K and 19 K, for the bulkPAA, the PAAsGOhwt and the PAAGOhwt systems, respectively. The estimated T_g value for the bulk PAA was found to be higher compared to the experimentally reported value (around 401 K[56]). This discrepancy could be attributed to the uncertainty introduced by the evaluated modulus data, as well as to the different cooling rates. The dynamical properties associated with the above mechanical behavior, will be studied, in the next section, with the use of eq. 1 and the fixed T_g and δ_g parameters determined from the above-described procedure.

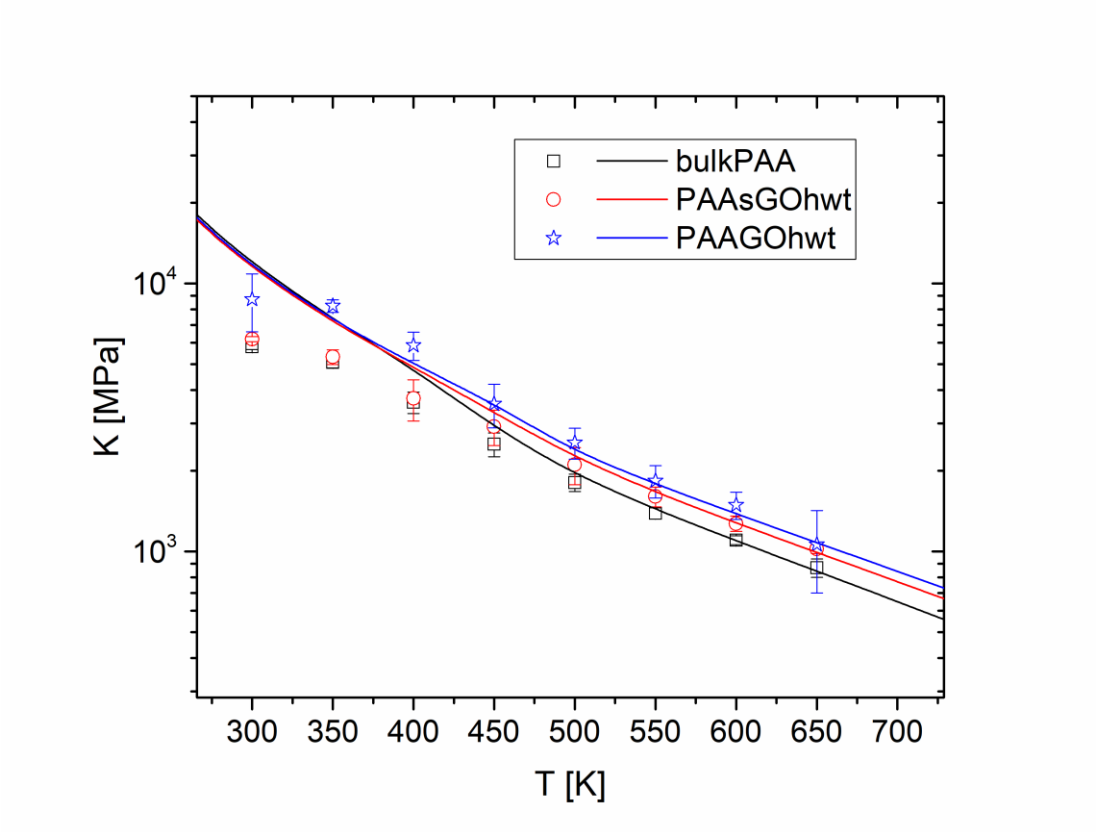

Figure 3. Bulk modulus (K) for the bulkPAA, PAAsGOhwt and PAAGOhwt systems, as evaluated by the volume fluctuations (symbols) and the SLG-model (eq. 4), (solid lines).

Based on the SLG-EoS, the thermal expansion coefficient, $a = -\frac{1}{\tilde{\rho}}\frac{\partial \tilde{\rho}}{\partial T}$, can be calculated by the expression:

$$a = \frac{\dot{\chi}\tilde{\rho}^2 - \frac{Pv}{kT^2}}{\tilde{\rho}\left(1-\frac{1}{r}\right) - \tilde{\rho}\left(\frac{1}{1-\tilde{\rho}}\right) + 2\chi\tilde{\rho}^2}, \quad (5)$$

where $\dot{\chi} = {}^{\partial \chi}/_{\partial T}$ (given in eq. s2 in SI). In Figure 4, we present (with solid lines) the predictions of eq. 5 for the α coefficient, for the bulk and the two nanocomposite systems. Also, with the black dash line, the estimation of α (bulkPAA) from the original SL model,[72] is depicted, allowing a comparison between the two models. It can be observed that at high temperatures (above 600 K) the two approaches practically converge to the same behavior, for the pure polymer. But at lower

temperatures a notable divergence is observed which becomes more pronounced when the glass transition is approached. Since the SLG-EoS describes accurately the temperature dependence of the density, it is reasonable to assume that the experimental behavior of α, at the glass transition region, would also follow the behavior predicted by eq. 5 (solid lines), which was derived based on eq. 3. Moreover, as depicted in Figure S3 of SI, this temperature dependence of the α coefficient leads to the prediction of a heat capacity step, in line with relevant experimental observations.[16,17,19]

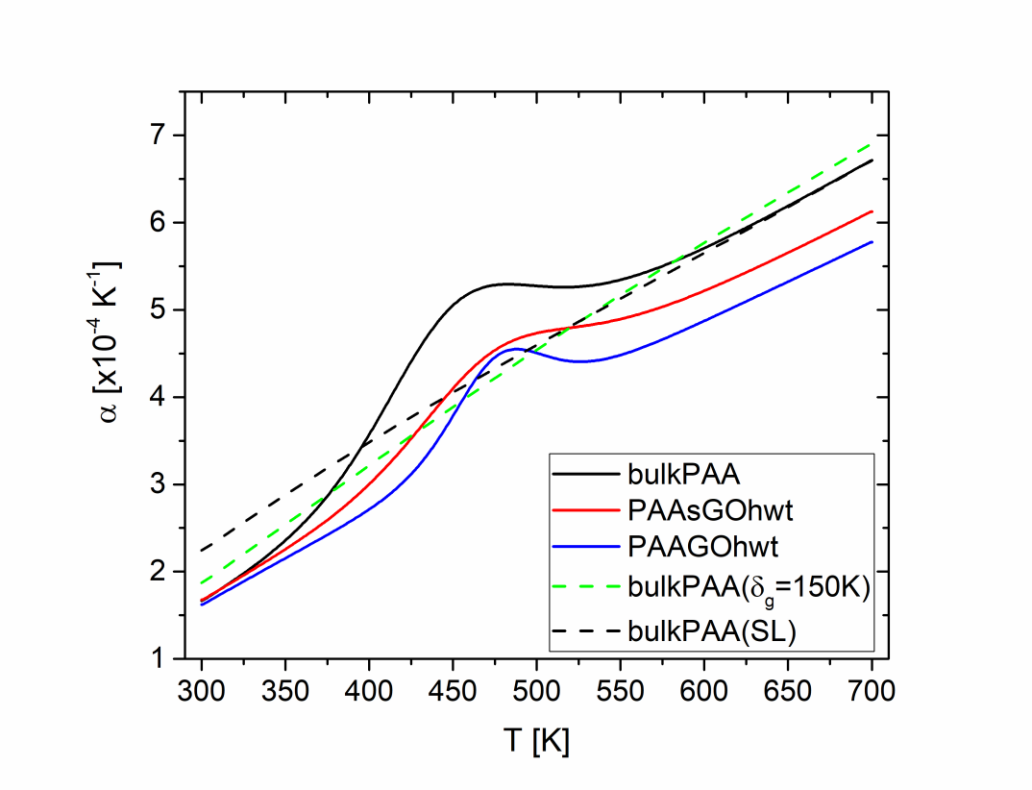

Figure 4. Thermal expansion coefficient (α), as described by the SLG model (solid lines) for the bulkPAA, PAAsGOhwt and the PAAGOhwt systems. The black dashed line corresponds to the description by the SL model and the green dashed line to a prediction of the SLG model (eq. 5), at δ_g=150 K, for the bulkPAA.

According to the SLG model, far below the T_g the thermal expansion coefficient follows the vanishing trend of the heat capacity. As the temperature rises, the solid state vibration continuously transforms to the confined, Arrhenius dynamics,[51,52] characterized by moderate values of α, close to $2x10^{-4}$ K^{-1}. Around the T_g region the cooperative diffusion comes at work, and the coefficient rises steeply, while at temperatures well above T_g, a plateau region, with an extent of almost 100 K, develops. At temperatures around 150 K above T_g, the SLG description recovers the behavior predicted by the SL theory, according which the entire system resides within the liquid state, $T^* = T_2^*$. Also, in case that we assume a rather broad region within which the super Arrhenius is extended (i.e., if we take δ_g =150 K), the thermal expansion coefficient follows an almost linear dependence with temperature (green dashed line in Figure. 4), similar the one predicted by the SL theory.

Regarding the morphological details of the chains belonging to the bound layer (see Figure 1), typical adsorbed configurations correspond to trains, loops, bridges and tails.[16,45] Trains consist of polymer atoms sequentially adsorbed on the surface, loops refer to non-adsorbed atoms, belonging to chain parts that emanate from the surface and are constrained by both ends, bridges are like loops, but with the two atoms restricting the chain part being adsorbed to different nanofillers and tails are chain parts where one end is free. Free, (i.e., non-adsorbed) chains, can be distinguished as well. The train's layer is identified with the adsorbed layer, while the bound layer is taken to include all chain configuration at the polymer/GO interfacial region (i.e, trains, loops, bridges and tails).

The probability of finding an atom of a chain in one of the above configurations is portrayed in Figure 5, as a function of the distance from the surface for both PAAsGOhwt and PAAGOhwt systems. It should be noted that atoms whose projection on the xy plane does not belong on the examined nanosheet, are not taken into account.

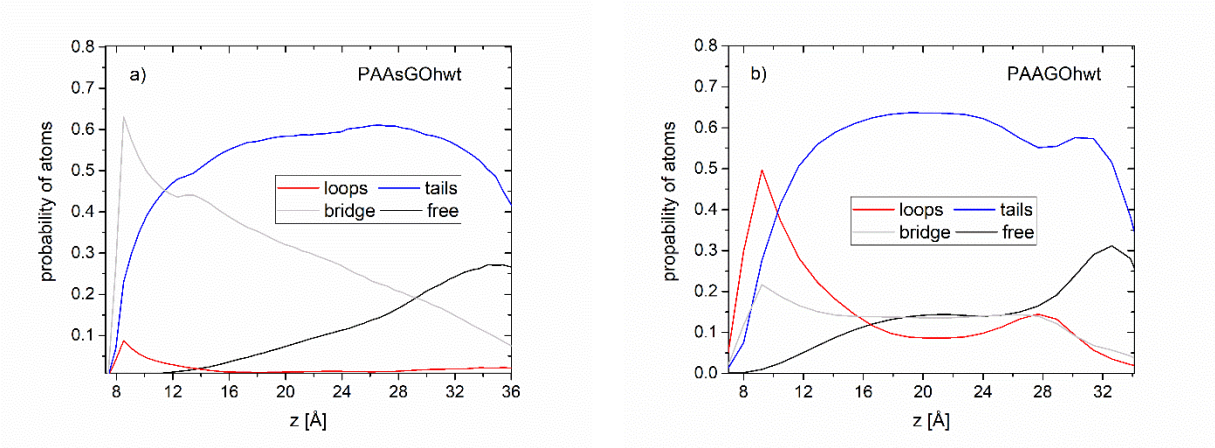

Figure 5. Probability for an atom to belong in one of the bound layer configurations as a function of its distance from the GO plane, for a) PAAsGOhwt and b) PAAGOhwt, at 600K.

It can be seen that the probability of finding loops, in the case of the small GO nanosheets, is rather low. On the other hand, in the large GO nanosheet system, the same probability is significantly higher, exhibiting a peak at a distance of 10 Å. Loops belonging to opposite nanosheets may overlap, explaining the non-zero values of the probability at the middle layer. It must also be mentioned that due to the presence of side groups in the PAA chain, even a sequentially adsorption of two successive side groups may result in the formation of a short loop. The distribution of the number of loops in each nanocomposite system is shown in Figure S4 of SI.

Tail configurations are dominant in both PAAsGOhwt and PAAGOhwt systems. The probability of this configuration appears to be almost the same, irrespectively of the GO size. On the contrary, the bridges prevail in the small GO system. Although, in the PAAGOhwt system the (z) box dimension is rather short (Figure S1 of SI) and was chosen close to the end-to-end distance of the chain (3.43 nm), it has been demonstrated[16] that even in the presence of strong polymer-filler interactions (e.g., hydrogen bonds), bridges of stretched chains with a pronounced divergence from

the random walk distance, are not favorable. Furthermore, the presence of free chains in both systems is not very frequent, and is more scarce in the PAAsGOhwt system. The probability of trains is equal to 1 within the adsorbed layer and zero elsewhere.

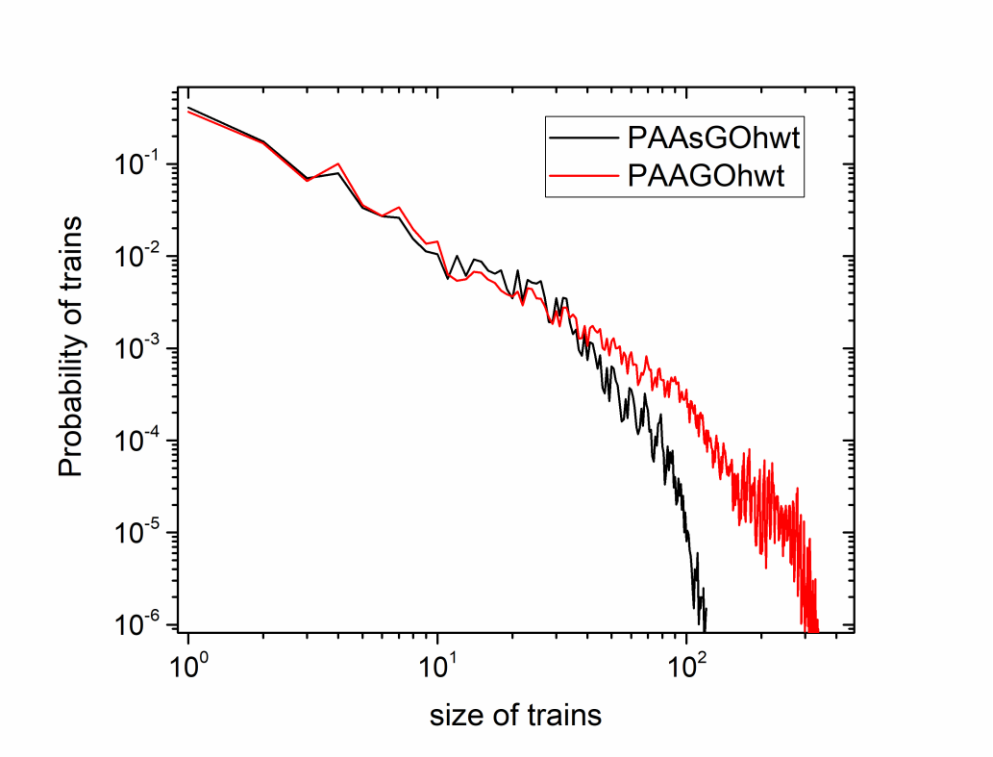

Figure 6. Probability of finding sequentially adsorbed atoms (trains' size) on the GO plane for the PAAsGOhwt and PAAGOhwt systems, at 500K.

The distribution of trains' size is shown in Figure 6. The formation of long trains, consisting of a large number of sequentially adsorbed chain atoms, could be taken as an indication of strong adhesion between PAA and GO. As anticipated, due to the larger size of the nanosheet, the longest trains are formed in the PAAGOhwt system. In both systems, the highest probability corresponds to the short trains of almost 2 atoms.[40]

Chain Dynamics and Enhanced Mechanical properties

Assuming the same mass, the two examined nanocomposite systems are characterized by the same polymer/GO interfacial area, but difference size of nanosheets. The ratios of the mean square displacement (MSD) for the center of mass (cm) of the polymer chains to the MSD of the cm for the GO, are shown in Figure 7, for a period of 30 ns. In the PAAsGOhwt system the small GOs are relatively mobile compared to the PAA chains resulting to an MSD ratio of the order of 1, while in case of the large GO nanosheet this ratio is of the order of 10. Also, it seems that in both cases the degree of dynamic decoupling between polymer chains and GO increases slightly (i.e., the ratios assume higher values) as the temperature rises. Comparison between the cm MSDs of the PAA and the GO is made in Figure S5 of SI. It can be inferred that a reduced mobility of the GO sheets, imparts slower average dynamics to the PAA chains due to the association between the two components.

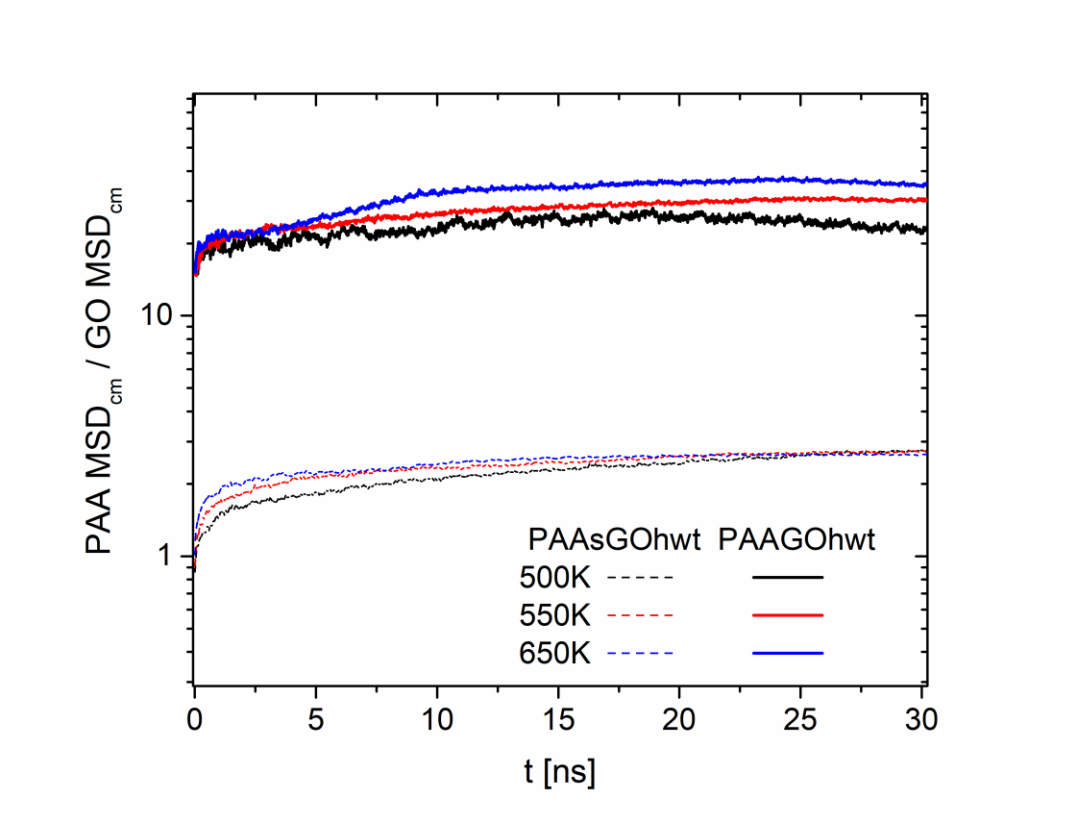

Figure 7. Ratio of the MSD of the cm for the PAA chains and the GO nanosheets, for the PAAsGOhwt and the PAAGOhwt systems, at various temperatures.

Figure 8, presents the desorption autocorrelation functions (ACFs) of PAA in the PAAsGOhwt and the PAAGOhwt systems. In addition, a comparison is made with the results presented in a previous study[28] for the PAAGOlwt system, referring to a large GO nanosheet under lower confinement conditions. The ACF curves are calculated based on the expression:

$$h(t) = \frac{\langle g(t)g(0)\rangle}{\langle g^2\rangle}, \quad (6)$$

where *g(t)* takes the value of 1, if at least one atom of the chain satisfies the adsorption criterion at time t and 0 otherwise.[28] Also, an extrapolation of the ACFs is possible through the mKKW function which combines a single and a stretched exponential fraction:[67,79]

$$P(t) = (1 - a_1)\exp\left[-\frac{t}{\tau_2}\right] + a_1\exp\left[-\left(\frac{t}{\tau_1}\right)^{\beta}\right] \quad (7)$$

The average decorrelation time τ_c, is calculated by the expression $\tau_c = (1 - \alpha_2)\tau_2 + a_1\left(\frac{\tau_1}{\beta}\right)\Gamma\left(\frac{1}{\beta}\right)$, where Γ is the Gamma function, $a_1$is the fraction of relaxation motions that are described by a stretched exponential (β parameter) and a characteristic time τ_1 and $(1 - a_1)$ represents the fraction of fast librational motions with exponential time dependence, with a characteristic time τ_2.

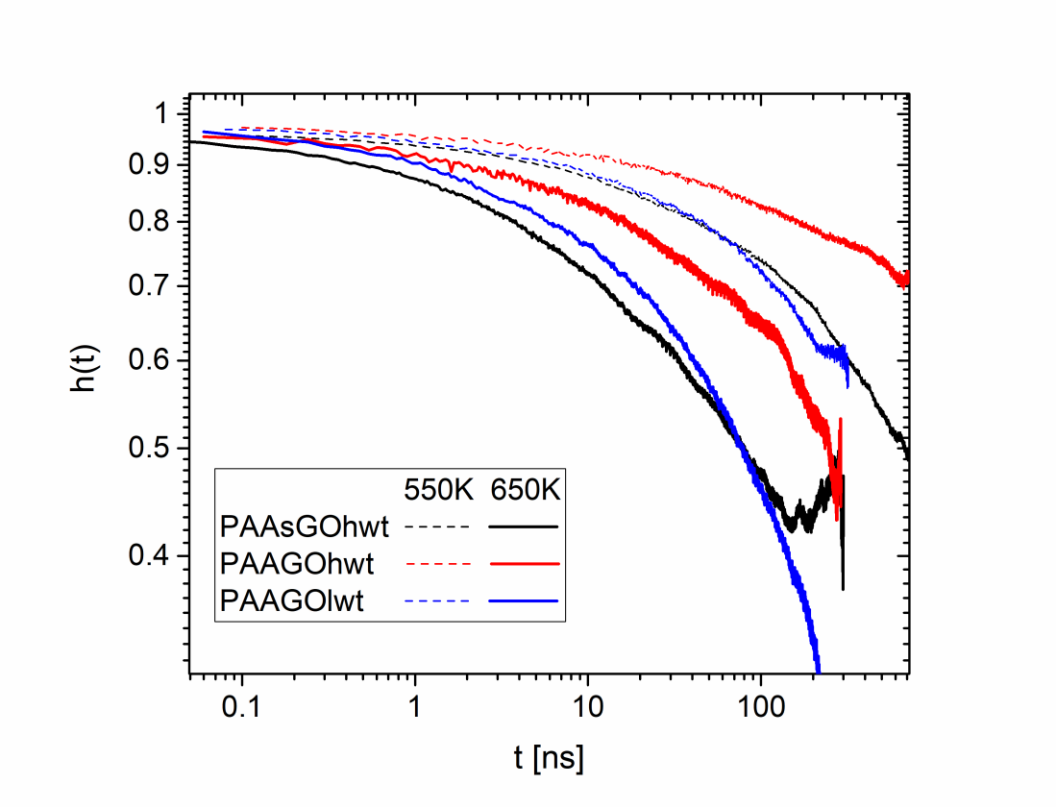

Figure 8. Desorption ACFs for the PAAsGOhwt, the PAAGOhwt and the PAAGOlwt systems, at 550 K and 650K.

The decorrelation times at 550 K and 650 K are evaluated (eq. 7) to be, for the PAAsGOhwt 42.0 x10^3 ns and 1.0 x10^3 ns, for the PAAGOhwt 1.2 x10^6 ns and 5.0 x 10^3 ns and for the PAAGOlwt 184.6x10^3 ns and 2.0 x10^3 ns, respectively. Comparing the estimated values for the PAAGOhwt and the PAAGOlwt systems, it becomes apparent that under strong confinement conditions a pronounced increase in the desorption time is observed. Furthermore, it can be concluded that the desorption of the chains from the small GO nanosheets is realized in a faster timescale compared to that characterizing the large GO flake. This can be accounted for, if we consider the train size distribution presented in Figure 6.

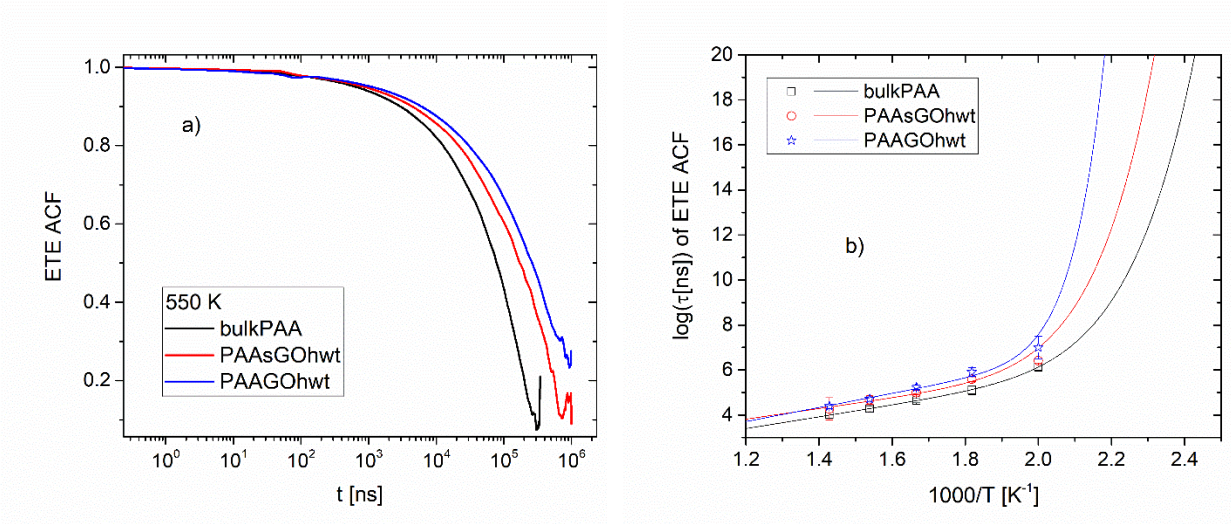

Figure 9. a) Chain end-to-end (ETE) vector ACFs, at 550 K and b) Arrhenius plots of the relaxation times of the ETE ACFs, for the bulkPAA, the PAAsGOhwt and the PAAGOhwt systems, calculated by eq. 7. The solid lines in (b) correspond to the fits according to the SLG model (eq. 1).

The effect of the GO mobility and the PAA desorption process on the chain dynamics can be studied through on the end-to-end vector ACFs, based on the first order Legendre polynomial ($P_1(t) = \langle \vec{e}(t) \cdot \vec{e}(0) \rangle$, with $\vec{e}$ being the unit vector). Figure 9a, displays such ACFs at 550 K for the two nanocomposite systems and the bulkPAA. The curves refer to an average behavior of PAA chains including either those in the free or in the adsorbed state. A clear trend of slower PAA dynamics in the system with the large GO can be observed. However, even at a temperature 100 K or more, above T_g, full decorrelation of the ACFs can not be attained. For this reason, based on eq. 1, an extrapolation of the high temperature behavior towards the entire super-Arrhenius region was performed, and the results are shown in the Arrhenius plot of Figure 9b. Since the simulation data are limited to five temperatures, the T_g and δ_g parameters were fixed, according to the thermodynamic analysis discussed earlier. Utilization of the SLG model allows the description of

dynamics in the entire region of cooperative diffusion, rendering much longer decorrelation times for the PAAGOhwt system, accompanied by an increased divergence between the times characterizing the two nanocomposites, at temperatures close to the respective T_g values.

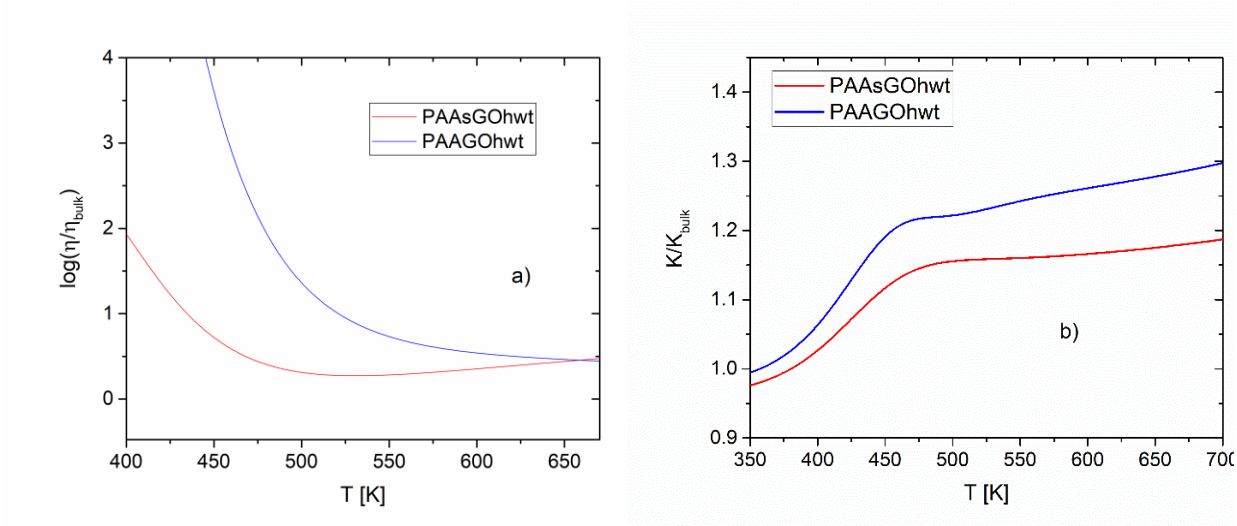

Figure 10. Normalized values with respect to bulk, for the two nanocomposite systems for a) the bulk modulus and b) the viscosity.

Quantification of the degree of enhancement in the mechanical properties in the two nanocomposites, is provided in Figure 10. Since the ratio (shift factor) of the end-to-end vector relaxation times (Figure 10a) can be considered close to the ratio of the viscosities, an approximation of the temperature dependence of the nanocomposite viscosity compared to the bulk can be attempted. An extrapolation of this ratio to the entire super Arrhenius region[51] confirms the enhanced mechanical behavior in the large GO systems. The ratio of the bulk modulus between each nanocomposite and the pristine polymer models is presented in Figure 10b. It can be inferred that the mechanical strength of both systems is enhanced compared to that of the pure polymer, while the PAAGOhwt system shows a higher modulus compared to that in the small GO system.

Segmental Dynamics

Decoupling of local dynamics in the adsorbed layer from that in the bulk, has previously been examined through the study of the mobility ratios.[28] A mobility ratio is defined as the weighted 2D atomic MSD component ($m_{xy}(t)$) within the bound layer, divided by the respective 3D component in the bulk ($m_{bulk}(t)$), i.e. $\frac{3m_{xy}(t)}{2m_{bulk}(t)}$. This analysis has recently been presented for various polymer/graphene nanocomposites and revealed a "cloaking" effect, where the influence of the presence of a GO sheet on local polymer dynamics was practically restricted within the adsorbed layer. A similar analysis is also presented here for the segmental dynamics within the adsorbed layer of the GO flakes in the two nanocomposites, and compared to that of the PAAGOlwt system,[28] as shown in Figure 11.

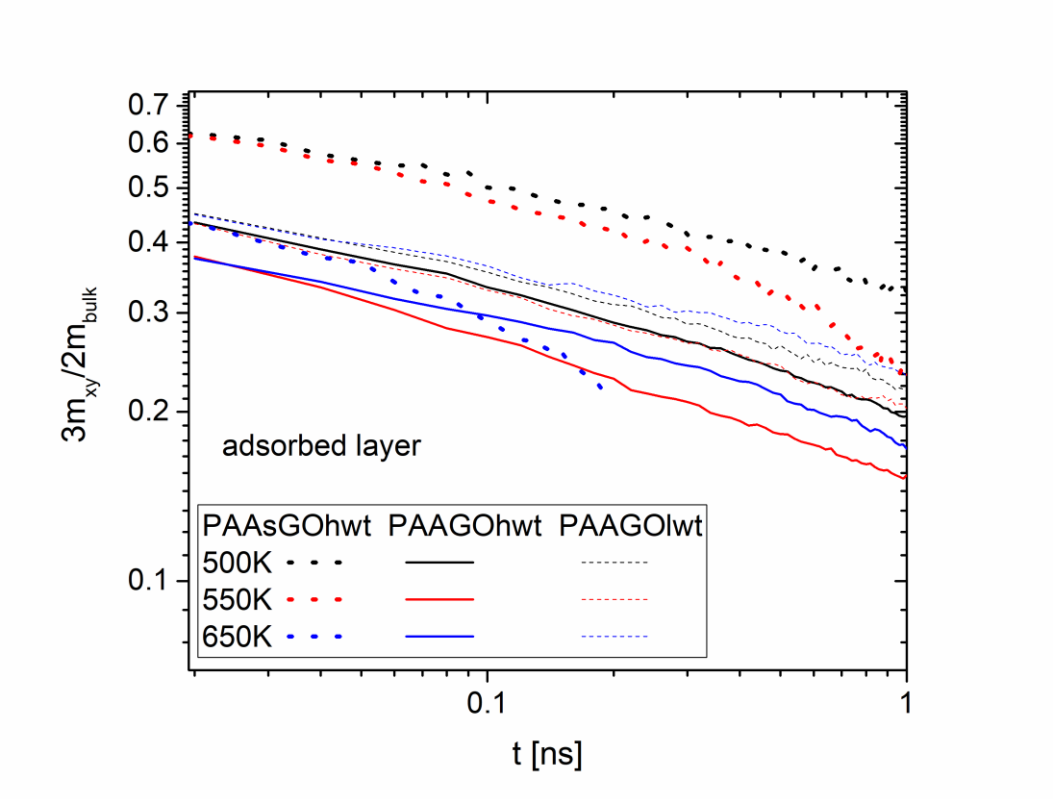

Figure 11. Time evolution of the xy mobility ratios, for the PAAsGOhwt, the PAAGOhwt and the PAAGOlwt systems, in the adsorbed layer, at various temperatures.

It is demonstrated that the strong confinement conditions of PAA between the large GO nanosheets, results in an enhanced decoupling behavior (i.e., lower mobility ratio values of the PAAGOhwt compared to those of PAAGOlwt). In other words, as the distance between the opposite nanosheets decreases, local dynamics in the bound layer becomes increasingly retarded. It can also be noted that in the small GO system, the mobility ratio varies within a wider range as temperature decreases, compared to that observed in the large GO systems. For instance, in the PAAsGOhwt, at T=650 K and t=20ps the ratio takes a value of 0.43, while at the same timescale and T=500 K, it rises to 0.63. On the other hand, for the PAAGOhwt the respective values range between 0.37 and 0.43. It should be mentioned that in the small GO system, at T=650 K, the statistics at long times are poor due to the fast desorption process of the chains. The effects of the GO size and the different degrees of confinement experienced by the polymer atoms close to the bound layer, are also reflected on the degree of dynamic heterogeneity of the atomic motion, as this is expressed by the non-Gaussian parameter.[28] Figure S6 of SI, portrays the stronger non-Gaussian nature of the atomic motion in a layer adjacent to the adsorbed layer in the nanocomposites compared to that of the bulk, and the higher degree of non-Gaussianity in the PAAGOhwt system.

Apart from the layer-based analysis, also adopted in similar simulations,[10,28] an alternative approach is to categorize local dynamics depending on the chain configurations within the bound layer, i.e. trains, loops, tails and bridges. According to this approach, bond reorientational dynamic motion is distinguished depending on the kind of chain configuration each bond belongs in, at the time origin t_0 and the examined time t.[80] Figure 12 shows the orientational correlation functions, based on the second Legendre polynomial ($P_2(t) = \frac{1}{2}\langle 3[\vec{e}(t) \cdot \vec{e}(0)]^2 - 1\rangle$, with $\vec{e}$ being the unit vector along the examined bond), of polymer carbon-carbon backbone bonds at T=600 K. The

relative degree of decorrelation of the corresponding ACFs show that bond orientational relaxation is somewhat slower in the adsorbed layer compared to that in the bulk, while effects related to the size of the GO filler, are also apparent. Namely, in the small GO system, the trains' ACF curve implies faster dynamics compared to the respective curve in the large GO system. Although the bridge configuration exhibits almost the same decorrelation rate in both systems, it is worth noticing that in the PAAsGOhwt system the divergence from the trains' dynamics is smaller, at high temperatures.

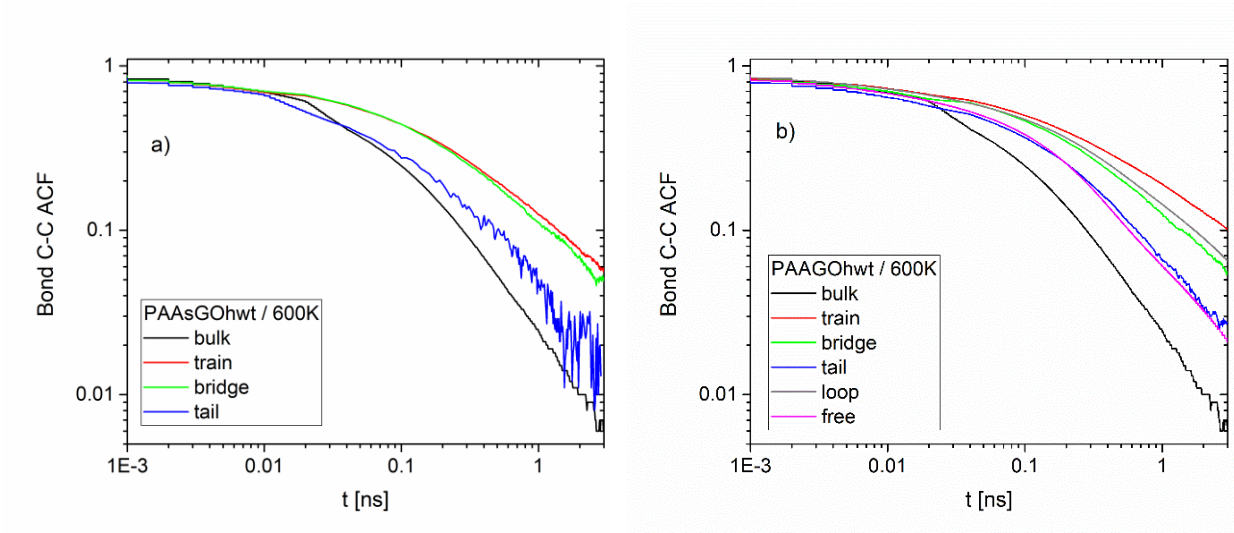

Figure 12. Bond relaxation ACFs for the backbone carbon-carbon (C-C) bond, in various bound layer configurations, for a) the PAAsGOhwt and b) the PAAGOhwt systems, at 600 K.

The temperature dependence of the bond relaxation times is shown in the activation plot of Figure 13. Extrapolation to the lower temperature range in made using eq. 1. In all cases, bonds belonging to configurations subjected to any kind of confinement, relax slower compared to the behavior seen in the bulk and in the free chains. In addition, dynamics of bonds belonging in the train configurations are slower, compared to that characterizing the rest of the configurations within the bound layer. It should also be noticed that the probability of loops and free chains in the

small GO system is rather low and so predictions about the relaxation times for those two configurations were not made.

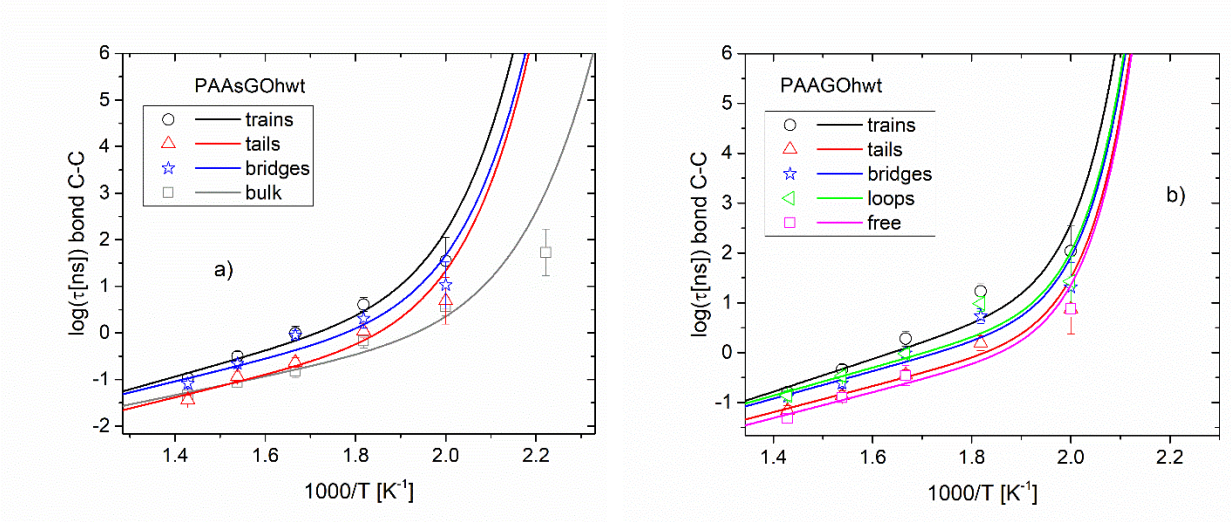

Figure 13. Arrhenius plots of the C-C bond relaxation times for the various bound layer configurations for a) the PAAsGOhwt and b) the PAAGOhwt systems. The solid lines correspond to the predictions of the SLG model.

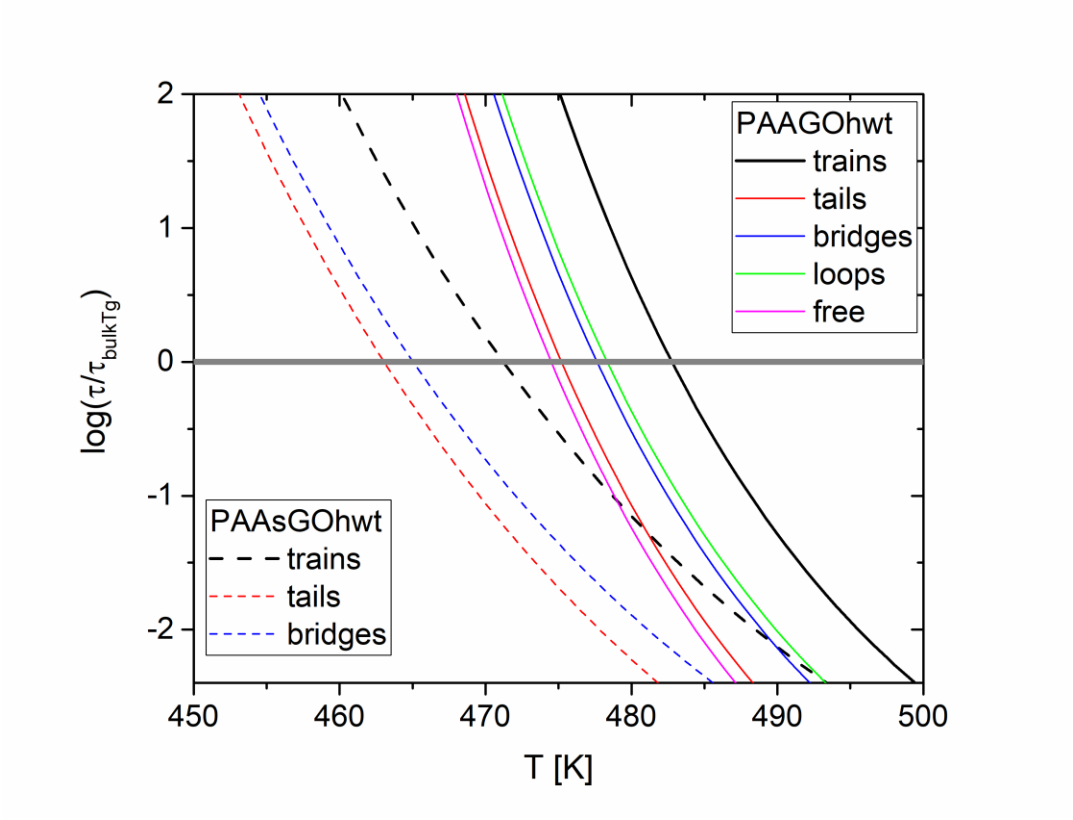

Figure 14. Immobilization (vitrification) temperature of the various bound layer configurations for both nanocomposite systems, as evaluated by the normalized super-Arrhenius curves (eq. 1) with respect to the bulk relaxation time at T_g (109.068 μs).

In order to determine the immobilization temperature (transition to a rigid amorphous phase[16]) of each configuration, in Figure 14, we present the relaxation times of the carbon-carbon backbone bonds, normalized with the value at T=T_g, of the bulk. When the logarithm of the ratio is equal to 0, immobilization (vitrification) of the configuration is assumed. For the first time, to our knowledge, configuration-resolved immobilization temperatures are determined from MD simulation results. It can clearly be seen that in both nanocomposite system the train configurations are dynamically arrested at higher temperatures. In the case of the PAAGOhwt system, configurational freezing-in of bonds belonging in train configurations, takes place at 485 K, almost 50 K above the bulk T_g, while for the PAAsGOhwt system the analogous difference is

almost 35 K. As for the rest configurations, their immobilization temperatures are close to the respective nanocomposite system's T_g and this attests to the dynamic decoupling, i.e, the cloaking effect.[27,28] It is worth noting that the loops, which represent a significant fraction of the bound layer in the large GO system, exhibit the slowest dynamics among the rest (excluding the trains) configurations. A similar study of loops in poly(butadiene)/Silica system,[28] revealed that the deceleration of the loops' dynamics is associated with the size of the loops, which is related to the size (r) of the chain. Longer chains form longer loops, which are distributed further from the surface and are characterized by less restricted dynamics. In general, at higher molecular weights the decoupling between the trains' layer and the rest bound layer fraction is expected to be more pronounced, explaining the trend of a stabilization in the T_g compared to the bulk.[13,14,17,24,29]

The picture emerging from the analysis above, is consistent with the ideas introduced in the framework of the SLG model, which already assumes the existence of immobilized segmental droplets. According to the presented analysis, under extreme confinement conditions, those droplets of immobilized segments, should mainly be related to the train configurations located on the adsorbed layer. After that, a density depletion layer is present (Figure 2b). At the interface the cooperativity is expressed as a strong decoupling between the adsorbed and the depletion layer.[28] Especially in the experimentally used, larger and less diffusible nanofillers,[2] the immobilization process may start earlier, at even higher temperatures, compared to the respective polymer T_g, justifying thus an extension of the super-Arrhenius region (δ_g parameter, of the order of 100 K) and an Arrhenius-like behavior.[51] It should be mentioned that under strong confinement conditions, the deformation of the depletion layer,[55] contributes to the enhanced values in the elastic modulus of polymer nanocomposites.

Although, the picture associated with the mechanism of mechanical reinforcement in polymer graphene nanocomposites is not complete yet, the present study showed that in the case of nanocomposites bearing the same interfacial area, the size and mobility of the nanosheet plays a significant role,[2,39,55] since it essentially controls polymer viscosity through the behavior at the bound layer. It should be emphasized that in our study neither "glassy polymer bridges" between nanofillers, nor strong filler-filler association, that could provide an alternative explanation for the enhanced mechanical properties of the nanocomposites, were observed.

Conclusions

Two PAA/GO nanocomposite systems characterized by the same mass fraction and different size nanosheets, have been studied by means of MD simulations. The present investigation considered also the effects of the chain configurations (i.e. trains, loops, tails and bridges), within the bound layer on the filler surface. Combination of results from fully atomistic MD simulations with the SLG model, allowed for the first time the extension of the thermodynamic and the dynamic behavior in the entire super-Arrhenius region.

The structural analysis of the bound layer attributed higher fraction of bridges in the case of the system with the smaller GO flakes and higher fraction of loops in the case of the system with the larger GO sheets. The size of trains was bigger for the PAAGOhwt (with the larger GO flakes) system.

The density temperature dependence and the change in the slope of the specific volume was described satisfactorily by the SLG-EoS. The bulk modulus behavior was formulated by a new equation (eq. 4). Using this formulation, stronger mechanical properties were detected for the PAAGOhwt system. Moreover, it was made possible to describe all the thermodynamic and dynamic properties with the same, fixed set of SLG parameters. The thermal expansion coefficient

equation that was derived, incorporated the glass transition and the description it provided was compatible with the experimental observation of a heat capacity step.

Concerning the dynamics, it was concluded that besides the width of the interfacial area and the strength of the polymer-filler interactions at the interphase, another significant parameter is the mobility of the nanosheet. In the system with the large GO sheets, the longer desorption process and the slower mobility on the adsorbed layer, imparted a higher increase in the viscosity of the nanocomposite, resulting in improved mechanical properties. The segmental dynamic analysis based on the type of the bound layer configurations, revealed that as the temperature drops, the immobilization of the trains' layer is always earlier (i.e., at higher temperature) providing a kind of nanofiller coating (shielding effect). The rest bound layer fraction exhibits decoupling characteristics and justifies the reduced heat capacity step at the nanocomposite's T_g.

The results described in this work indicate that in the super-Arrhenius region, the density, along with the dynamic and mechanical behavior can be described with the use of one T_g parameter. A new methodology, combining MD simulations and the thermodynamic SLG EoS-based model, is proposed for the characterization of glassy materials.

ASSOCIATED CONTENT

In the Supporting Information we present, Figure S1 with snapshots of the whole nanocomposite systems, Figure S2 with the temperature dependence of the density, Figure S3 with the temperature dependence of the heat capacity, Figure S4 with the distribution of the number of loops in each nanosheet, Figure S5 with the MSD of the cm of PAA and GO, Figure S6 with the non-Gaussian parameter, Table S1 with the fitting parameters to the SLG-EoS and Tables S2-S5 with the fitting parameters to eq.1. Moreover eqs. S1 and S2 are also depicted.

AUTHOR INFORMATION

Corresponding Authors

*Email: kritikgio@gmail.com

References

(1) Hamed, G. R.; Hatfield, S. On the Role of Bound Rubber in Carbon-Black Reinforcement. *Rubber Chem. Technol.* **1989**, *62* (1), 143–156.

(2) Anagnostopoulos, G.; Androulidakis, C.; Koukaras, E. N.; Tsoukleri, G.; Polyzos, I.; Parthenios, J.; Papagelis, K.; Galiotis, C. Stress Transfer Mechanisms at the Submicron Level for Graphene/Polymer Systems. *ACS Appl. Mater. Interfaces* **2015**, *7* (7), 4216–4223.

(3) Young, R. J.; Kinloch, I. A.; Gong, L.; Novoselov, K. S. The Mechanics of Graphene Nanocomposites: A Review. *Compos. Sci. Technol.* **2012**, *72* (12), 1459–1476.

(4) Karatrantos, A. V.; Clarke, N. Polymer Dynamics in Polymer-Nanoparticle Interface. In *Springer Series in Materials Science*; Springer, Cham, 2021; Vol. 310, pp 81–100.

(5) Cangialosi, D.; Boucher, V. M.; Alegría, A.; Colmenero, J. Enhanced Physical Aging of Polymer Nanocomposites: The Key Role of the Area to Volume Ratio. *Polymer (Guildf).* **2012**, *53* (6), 1362–1372.

(6) Fragiadakis, D.; Pissis, P. Glass Transition and Segmental Dynamics in Poly(Dimethylsiloxane)/Silica Nanocomposites Studied by Various Techniques. *J. Non. Cryst. Solids* **2007**, *353* (47–51), 4344–4352.

(7) Priestley, R. D.; Rittigstein, P.; Broadbelt, L. J.; Fukao, K.; Torkelson, J. M. Evidence for the Molecular-Scale Origin of the Suppression of Physical Ageing in Confined Polymer: Fluorescence and Dielectric Spectroscopy Studies of Polymer–Silica Nanocomposites. *J. Phys. Condens. Matter* **2007**, *19* (20), 205120.

(8) Starr, F. W.; Schroeder, T. B.; Glotzer, S. C. Molecular Dynamics Simulation of a Polymer Melt with a Nanoscopic Particle. *Macromolecules* **2002**, *35* (11), 4481–4492.

(9) Jimenez, A. M.; Zhao, D.; Misquitta, K.; Jestin, J.; Kumar, S. K. Exchange Lifetimes of the Bound Polymer Layer on Silica Nanoparticles. *ACS Macro Lett.* **2019**, 166–171.

(10) Yelash, L.; Virnau, P.; Binder, K.; Paul, W. Slow Process in Confined Polymer Melts: Layer Exchange Dynamics at a Polymer Solid Interface. *Phys. Rev. E - Stat. Nonlinear, Soft Matter Phys.* **2010**, *82* (5), 050801.

(11) Kirst, K. U.; Kremer, F.; Litvinov, V. M. Broad-Band Dielectric Spectroscopy on the Molecular Dynamics of Bulk and Adsorbed Poly(Dimethylsiloxane). *Macromolecules* **1993**, *26* (5), 975–980.

(12) Anastasiadis, S. H.; Karatasos, K.; Vlachos, G.; Manias, E.; Giannelis, E. P. Nanoscopic-Confinement Effects on Local Dynamics. *Phys. Rev. Lett.* **2000**, *84* (5), 915–918.

(13) Baeza, G. P.; Dessi, C.; Costanzo, S.; Zhao, D.; Gong, S.; Alegria, A.; Colby, R. H.; Rubinstein, M.; Vlassopoulos, D.; Kumar, S. K. Network Dynamics in Nanofilled Polymers. *Nat. Commun.* **2016**, *7*, 11368.

(14) Xu, H.; Song, Y.; Jia, E.; Zheng, Q. Dynamics Heterogeneity in Silica-Filled Nitrile Butadiene Rubber. *J. Appl. Polym. Sci.* **2018**, *135* (22), 63–67.

(15) Barut, G.; Pissis, P.; Pelster, R.; Nimtz, G. Glass Transition in Liquids: Two versus Three-Dimensional Confinement. *Phys. Rev. Lett.* **1998**, *80* (16), 3543–3546.

(16) Kritikos, G. Transition of the Bounded Polymer Layer to a Rigid Amorphous Phase: A Computational and DSC Study. *Polymer (Guildf).* **2014**, *55* (18), 4658–4670.

(17) Koutsoumpis, S.; Klonos, P.; Raftopoulos, K. N.; Papadakis, C. M.; Bikiaris, D.; Pissis, P. Morphology, Thermal Properties and Molecular Dynamics of Syndiotactic Polystyrene (s-PS) Nanocomposites with Aligned Graphene Oxide and Graphene Nanosheets. *Polymer (Guildf).* **2018**, *153*, 548–557.

(18) Şerbescu, A.; Saalwächter, K. Particle-Induced Network Formation in Linear PDMS Filled with Silica. *Polymer (Guildf).* **2009**, *50* (23), 5434–5442.

(19) Wunderlich, B. Reversible Crystallization and the Rigid-Amorphous Phase in Semicrystalline Macromolecules. *Prog. Polym. Sci.* **2003**, *28* (3), 383–450.

(20) Napolitano, S.; Wübbenhorst, M. The Lifetime of the Deviations from Bulk Behaviour in Polymers Confined at the Nanoscale. *Nat. Commun.* **2011**, *2* (1), 260.

(21) Koga, T.; Jiang, N.; Gin, P.; Endoh, M. K.; Narayanan, S.; Lurio, L. B.; Sinha, S. K. Impact of an Irreversibly Adsorbed Layer on Local Viscosity of Nanoconfined Polymer Melts. *Phys. Rev. Lett.* **2011**, *107* (22), 225901.

(22) Del Río, J.; Etxeberria, A.; López-Rodríguez, N.; Lizundia, E.; Sarasua, J. R. A PALS Contribution to the Supramolecular Structure of Poly(l -Lactide). *Macromolecules* **2010**, *43* (10), 4698–4707.

(23) Jimenez, A. M.; Altorbaq, A. S.; Muller, A. J.; Kumar, S. K. Polymer Crystallization under Confinement by Well-Dispersed Nanoparticles. *Macromolecules* **2020**, *53* (22), 10256–10266.

(24) Wurm, A.; Ismail, M.; Kretzschmar, B.; Pospiech, D.; Schick, C. Retarded Crystallization in Polyamide/Layered Silicates Nanocomposites Caused by an Immobilized Interphase. *Macromolecules* **2010**, *43* (3), 1480–1487.

(25) Papananou, H.; Perivolari, E.; Chrissopoulou, K.; Anastasiadis, S. H. Tuning Polymer Crystallinity via the Appropriate Selection of Inorganic Nanoadditives. *Polymer (Guildf).* **2018**, *157*, 111–121.

(26) Kritikos, G.; Terzis, A. F. Variable Density Self Consistent Field Study on Bounded Polymer Layer around Spherical Nanoparticles. *Eur. Polym. J.* **2013**, *49* (3), 613–629.

(27) Starr, F. W.; Douglas, J. F.; Meng, D.; Kumar, S. K. Bound Layers "Cloak" Nanoparticles in Strongly Interacting Polymer Nanocomposites. *ACS Nano* **2016**, *10* (12), 10960–10965.

(28) Kritikos, G.; Rissanou, A. N.; Harmandaris, V.; Karatasos, K. Bound Layer Polymer Behavior on Graphene and Graphene Oxide Nanosheets. *Macromolecules* **2020**, *53* (15), 6190–6203.

(29) Klonos, P.; Panagopoulou, A.; Bokobza, L.; Kyritsis, A.; Peoglos, V.; Pissis, P. Comparative Studies on Effects of Silica and Titania Nanoparticles on Crystallization and Complex Segmental Dynamics in Poly(Dimethylsiloxane). *Polymer (Guildf).* **2010**, *51* (23), 5490–5499.

(30) Bansal, A.; Yang, H.; Li, C.; Cho, K.; Benicewicz, B. C.; Kumar, S. K.; Schadler, L. S. Quantitative Equivalence between Polymer Nanocomposites and Thin Polymer Films. *Nat. Mater.* **2005**, *4* (9), 693–698.

(31) Zhu, Z.; Thompson, T.; Wang, S. Q.; Von Meerwall, E. D.; Halasa, A. Investigating Linear and Nonlinear Viscoelastic Behavior Using Model Silica-Particle-Filled Polybutadiene. *Macromolecules* **2005**, *38* (21), 8816–8824.

(32) Merabia, S.; Sotta, P.; Long, D. R. A Microscopic Model for the Reinforcement and the Nonlinear Behavior of Filled Elastomers and Thermoplastic Elastomers (Payne and Mullins Effects). *Macromolecules* **2008**, *41* (21), 8252–8266.

(33) Maier, P. G.; Goritz, D. Molecular Interpretation of the Payne Effect. *Kautsch. Gummi Kunstst.* **1996**, *49* (1), 18–21.

(34) De Gennes, P. G. Glass Transitions in Thin Polymer Films. *Eur. Phys. J. E* **2000**, *2* (3), 201–205.

(35) Tsagaropoulos, G.; Eisenberg, A. Direct Observation of Two Glass Transition in Silica-Filled Polymers. Implications for the Morphology of Random Ionomers. *Macromolecules* **1995**, *28* (1), 396–398.

(36) Payne, A. R. Dynamic Properties of Heat-treated Butyl Vulcanizates. *J. Appl. Polym. Sci.* **1963**, *7* (3), 873–885.

(37) Mujtaba, A.; Keller, M.; Ilisch, S.; Radusch, H. J.; Beiner, M.; Thurn-Albrecht, T.; Saalwächter, K. Detection of Surface-Immobilized Components and Their Role in

Viscoelastic Reinforcement of Rubber-Silica Nanocomposites. *ACS Macro Lett.* **2014**, *3* (5), 481–485.

(38) Behbahani, A. F.; Vaez Allaei, S. M.; Motlagh, G. H.; Eslami, H.; Harmandaris, V. A. Structure, Dynamics, and Apparent Glass Transition of Stereoregular Poly(Methyl Methacrylate)/Graphene Interfaces through Atomistic Simulations. *Macromolecules* **2018**, *51* (19), 7518–7532.

(39) Emamy, H.; Kumar, S. K.; Starr, F. W. Structural Properties of Bound Layer in Polymer-Nanoparticle Composites. *Macromolecules* **2020**, *53* (18), 7845–7850.

(40) Behbahani, A. F.; Rissanou, A.; Kritikos, G.; Doxastakis, M.; Burkhart, C.; Polińska, P.; Harmandaris, V. A. Conformations and Dynamics of Polymer Chains in Cis and Trans Polybutadiene/Silica Nanocomposites through Atomistic Simulations: From the Unentangled to the Entangled Regime. *Macromolecules* **2020**, *53* (15), 6173–6189.

(41) Brown, D.; Mélé, P.; Marceau, S.; Albérola, N. D. A Molecular Dynamics Study of a Model Nanoparticle Embedded in a Polymer Matrix. *Macromolecules* **2003**, *36* (4), 1395–1406.

(42) Papakonstantopoulos, G. J.; Yoshimoto, K.; Doxastakis, M.; Nealey, P. F.; De Pablo, J. J. Local Mechanical Properties of Polymeric Nanocomposites. *Phys. Rev. E - Stat. Nonlinear, Soft Matter Phys.* **2005**, *72* (3), 1–6.

(43) Sgouros, A. P.; Vogiatzis, G. G.; Kritikos, G.; Boziki, A.; Nikolakopoulou, A.; Liveris, D.; Theodorou, D. N. Molecular Simulations of Free and Graphite Capped Polyethylene Films: Estimation of the Interfacial Free Energies. *Macromolecules* **2017**, *50* (21), 8827–8844.

(44) Daoulas, K. C.; Harmandaris, V. A.; Mavrantzas, V. G. Detailed Atomistic Simulation of a Polymer Melt/Solid Interface: Structure, Density, and Conformation of a Thin Film of Polyethylene Melt Adsorbed on Graphite. *Macromolecules* **2005**, *38* (13), 5780–5795.

(45) Scheutjens, J. M. H. M.; Fleer, G. J. Statistical Theory of the Adsorption of Interacting Chain Molecules. 2. Train, Loop, and Tail Size Distribution. *J. Phys. Chem.* **1980**, *84* (2), 178–190.

(46) Vogel, H. The Temperature Dependence Law of the Viscosity of Fluids. *Phys. Zeit.* **1921**, *22*, 645–646.

(47) Tammann, G.; Hesse, W. The Dependancy of Viscosity on Temperature in Hypothermic Liquids. *Z. Anorg. Allg. Chem.* **1926**, *156*, 245–257.

(48) Fulcher, G. S. Analysis of Recent Measurments of the Viscosity of Glasses. *J. Am. Ceram. Soc.* **1925**, *8* (6), 339–355.

(49) Schmidtke, B.; Hofmann, M.; Lichtinger, A.; Rössler, E. A. Temperature Dependence of the Segmental Relaxation Time of Polymers Revisited. *Macromolecules* **2015**, *48* (9), 3005–3013.

(50) Stickel, F.; Fischer, E. W.; Richert, R. Dynamics of Glass-Forming Liquids. I. Temperature-Derivative Analysis of Dielectric Relaxation Data. *J. Chem. Phys.* **1995**, *102* (15), 6251–

6257.

(51) Kritikos, G. Exploring a Unified Description of the Super-Arrhenius Region above and below the Glass Transition Temperature. *Soft Matter* **2020**, *16*, 6902–6913.

(52) Johari, C. P.; Goldstein, M. Viscous Liquids and the Glass Transition. II. Secondary Relaxations in Glasses of Rigid Molecules. *J. Chem. Phys.* **1970**, *53* (6), 2372–2388.

(53) Hecksher, T.; Nielsen, A. I.; Olsen, N. B.; Dyre, J. C. Little Evidence for Dynamic Divergences in Ultraviscous Molecular Liquids. *Nat. Phys.* **2008**, *4* (9), 737–741.

(54) McKenna, G. B. Glass Dynamics: Diverging Views on Glass Transition. *Nat. Phys.* **2008**, *4* (9), 673–674.

(55) Kritikos, G.; Karatasos, K. Temperature Dependence of Dynamic and Mechanical Properties in Poly(Acrylic Acid)/Graphene Oxide Nanocomposites. *Mater. Today Commun.* **2017**, *13* (October), 359–366.

(56) Kritikos, G. Mean Field Description of the Structural Heterogeneities in the Region of Cooperative Diffusion. *Comput. Mater. Sci.* **2020**, *179*, 109682.

(57) Karatasos, K.; Kritikos, G. Characterization of a Graphene Oxide/Poly(Acrylic Acid) Nanocomposite by Means of Molecular Dynamics Simulations. *RSC Adv.* **2016**, *6* (111), 109267–109277.

(58) *Polymer-Graphene Nanocomposites*; Mittal, V., Ed.; Nanoscience & Nanotechnology Series; Royal Society of Chemistry: Cambridge, 2012.

(59) Stauffer, D.; Dragneva, N.; Floriano, W. B.; Mawhinney, R. C.; Fanchini, G.; French, S.; Rubel, O. An Atomic Charge Model for Graphene Oxide for Exploring Its Bioadhesive Properties in Explicit Water. *J. Chem. Phys.* **2014**, *141* (4), 044705.

(60) Cornell, W. D.; Cieplak, P.; Bayly, C. I.; Gould, I. R.; Merz, K. M.; Ferguson, D. M.; Spellmeyer, D. C.; Fox, T.; Caldwell, J. W.; Kollman, P. A. A Second Generation Force Field for the Simulation of Proteins, Nucleic Acids, and Organic Molecules. *J. Am. Chem. Soc.* **1995**, *117* (19), 5179–5197.

(61) Wang, J. M.; Wolf, R. M.; Caldwell, J. W.; Kollman, P. a; Case, D. a. Development and Testing of a General Amber Force Field. *J. Comput. Chem.* **2004**, *25* (9), 1157–1174.

(62) Hess, B.; Kutzner, C.; Van Der Spoel, D.; Lindahl, E. GROMACS 4: Algorithms for Highly Efficient, Load-Balanced, and Scalable Molecular Simulation. *J. Chem. Theory Comput.* **2008**, *4* (3), 435–447.

(63) Bussi, G.; Donadio, D.; Parrinello, M. Canonical Sampling through Velocity Rescaling. *J. Chem. Phys.* **2007**, *126* (1), 014101.

(64) Berendsen, H. J. C.; Postma, J. P. M.; Van Gunsteren, W. F.; Dinola, A.; Haak, J. R. Molecular Dynamics with Coupling to an External Bath. *J. Chem. Phys.* **1984**, *81* (8), 3684–3690.

(65) Wood, W. W.; Jacobson, J. D. Preliminary Results from a Recalculation of the Monte Carlo Equation of State of Hard Spheres. *The Journal of Chemical Physics*. 1957, pp 1207–1208.

(66) Alder, B. J.; Wainwright, T. E. Phase Transition for a Hard Sphere System. *The Journal of Chemical Physics*. 1957, pp 1208–1209.

(67) Ngai, K. L. *Relaxation and Diffusion in Complex Systems*; Partially Ordered Systems; Springer New York, 2011.

(68) Flory, P. J. Thermodynamics of High Polymer Solutions. *J. Chem. Phys.* **1942**, *10* (1), 51–61.

(69) Huggins, M. L. Thermodynamic Properties of Solutions of Long-Chain Compounds. *Ann. N. Y. Acad. Sci.* **1942**, *43* (1), 1–32.

(70) Biroš, J.; Zeman, L.; Patterson, D. Prediction of the x Parameter by the Solubility Parameter and Corresponding States Theories. *Macromolecules* **1971**, *4* (1), 30–35.

(71) Chremos, A.; Nikoubashman, A.; Panagiotopoulos, A. Z. Flory-Huggins Parameter χ, from Binary Mixtures of Lennard-Jones Particles to Block Copolymer Melts. *J. Chem. Phys.* **2014**, *140* (5).

(72) Sanchez, I. C.; Lacombe, R. H. Elementary Equation of State for Polymer Liquids. *J. Polym. Sci. Polym. Lett. Ed.* **1977**, *15* (2), 71–75.

(73) Balbuena, C.; Mariel Gianetti, M.; Rodolfo Soulé, E. A Structural Study and Its Relation to Dynamic Heterogeneity in a Polymer Glass Former. *Soft Matter* **2021**, *17*, 3503–3512.

(74) Xu, W. S.; Douglas, J. F.; Xu, X. Role of Cohesive Energy in Glass Formation of Polymers with and without Bending Constraints. *Macromolecules* **2020**, *53* (22), 9678–9697.

(75) Humphrey, W.; Dalke, A.; Schulten, K. VMD: Visual Molecular Dynamics. *J. Mol. Graph.* **1996**, *14* (1), 33–38.

(76) Kritikos, G.; Pant, R.; Sengupta, S.; Karatasos, K.; Venkatnathan, A.; Lyulin, A. V. Nanostructure and Dynamics of Humidified Nafion/Graphene-Oxide Composites via Molecular Dynamics Simulations. *J. Phys. Chem. C* **2018**, *122* (40), 22864–22875.

(77) *Physical Properties of Polymers*; Mark, J. E., Ed.; Cambridge University Press, 2004.

(78) Nazarychev, V. M.; Lyulin, A. V.; Larin, S. V.; Gurtovenko, A. A.; Kenny, J. M.; Lyulin, S. V. Molecular Dynamics Simulations of Uniaxial Deformation of Thermoplastic Polyimides. *Soft Matter* **2016**, *12* (17), 3972–3981.

(79) Alvarez, F.; Alegra, A.; Colmenero, J. Relationship between the Time-Domain Kohlrausch-Williams-Watts and Frequency-Domain Havriliak-Negami Relaxation Functions. *Phys. Rev. B* **1991**, *44* (14), 7306–7312.

(80) Kritikos, G.; Sgouros, A.; Vogiatzis, G. G.; Theodorou, D. N. Molecular Dynamics Study of Polyethylene under Extreme Confinement. *J. Phys. Conf. Ser.* **2016**, *738* (1), 012012.

for Table of Contents use only

Effect of Nanofiller's Size on the Mechanical Properties of Poly(acrylic acid)/Graphene Oxide Nanocomposites

Georgios Kritikos and Kostas Karatasos*